



**HAL**  
open science

## Digital-Based Solution for the Generation of FM/PM Test Stimuli

Kamilia Tahraoui, Thibault Vayssade, François Lefèvre, Laurent Latorre,  
Florence Azaïs

► **To cite this version:**

Kamilia Tahraoui, Thibault Vayssade, François Lefèvre, Laurent Latorre, Florence Azaïs. Digital-Based Solution for the Generation of FM/PM Test Stimuli. IEEE Transactions on Computer-Aided Design of Integrated Circuits and Systems, In press, pp.1-1. 10.1109/TCAD.2024.3434356 . lirmm-04689470

**HAL Id: lirmm-04689470**

**<https://hal-lirmm.ccsd.cnrs.fr/lirmm-04689470v1>**

Submitted on 5 Sep 2024

**HAL** is a multi-disciplinary open access archive for the deposit and dissemination of scientific research documents, whether they are published or not. The documents may come from teaching and research institutions in France or abroad, or from public or private research centers.

L'archive ouverte pluridisciplinaire **HAL**, est destinée au dépôt et à la diffusion de documents scientifiques de niveau recherche, publiés ou non, émanant des établissements d'enseignement et de recherche français ou étrangers, des laboratoires publics ou privés.

# Digital-based solution for the generation of FM/PM test stimuli

K. Tahraoui, *Member, IEEE*, T. Vayssade, *Member, IEEE*, F. Lefèvre,  
L. Latorre, *Member, IEEE*, and F. Azaïs, *Member, IEEE*.

**Abstract**—This paper explores a low-cost solution for generating modulated test stimuli using a standard digital Automated Test Equipment (ATE). The technique relies on the generation of a modulated binary signal with appropriate encoding using a digital tester channel and the exploitation of one of its harmonic replicas. A theoretical analysis is presented in this paper, considering a simple modulation scheme, i.e. single-tone frequency or phase modulation. The relationship between the baseband spectrum and the harmonic replicas is established and an analytical expression of the modulated digital signal is derived, taking into account effects associated with discrete-time generation. A corruption estimator is then defined, enabling non-destructive sampling conditions to be identified. Experimental results are provided demonstrating the ability of the proposed solution to generate a modulated signal with the desired characteristics at a frequency higher than that of the test equipment.

**Index Terms**— Analog/RF test; test signal generation; digital ATE; sampling theory; frequency/phase modulation.

## I. INTRODUCTION

**B**ECAUSE of the intrinsic variability of the manufacturing processes, the quality and the performance of each individual microelectronic product must be thoroughly verified and characterized before selling. The test of silicon dies is done at several stages of the fabrication process to ensure that every chip meet its specifications, introducing costs that substantially contribute to the overall manufacturing expenses. For decades, research has been driven to lower these costs, early introducing the idea of structural testing. It eliminates the need for an exhaustive functional test that would be impossible to conduct anyway, considering the circuit complexity. While such approach is standard for digital circuits, analog and RF devices specifications are still verified by means of conventional performance measurements using a dedicated instrumentation.

In particular, wireless communications have become ubiquitous in several applications that include personal computing, smartphones, home appliances, health monitoring devices, WSN (Wireless Sensor Network) and IoT (Internet of Things) to name a few. At the heart of these communicating devices, we usually find a System on Chip (SoC) that embeds

computing resources together with an RF front-end and an associated standard protocol stack such as Wi-Fi, Bluetooth or Zigbee. It is a very competitive market where costs are squeezed at application level, urging silicon vendors to develop competitiveness by reducing their production expenses.

The physical layer of these RF devices is mostly based on a narrow-band modulation scheme such as FSK (Frequency-Shift Keying), PSK (Phase-Shift Keying) or one of their improved variants. RF specifications differs for transmitters (TX) and receivers (RX) so that even transceivers doing both can still be seen as two separate transmission paths, each requiring a dedicated test approach. Testing the TX path is done by analyzing the spectral content of the sourced RF signal and measuring its EVM (Error Vector Magnitude). Testing the RX path is mostly a functional test that verifies the correct reception of test data, in particular using a test signal with power level close to the receiver's minimum receivable power (typically -95dBm). In both cases, a dedicated RF instrumentation is required to generate or analyze high frequency modulated signals. Such instrumentation is expensive and represents a bottleneck in the batch production chain.

To reduce the testing costs, one approach is to develop solutions that relax constraints on the required instrumentation, so that a low-cost tester can be used. The ultimate aim is for this low-cost tester to be a digital tester, as this enables the digital part of an SoC to be tested using the same test infrastructure as the RF part. A number of research works can be found in the literature targeting the development of digital solutions, including the use of a reference transceiver accompanied by a FPGA to handle the interface between the transceiver and a digital ATE [1], the use of a processor embedded in a radio SoC to implement self-test and provide low-frequency digital output [2], or the proposal of an ATE architecture with multi-level drivers and comparators for direct modulation/demodulation of QAM signals [3]. Other works specifically target test response analysis using digital ATE channels, including analysis of modulated signals [4], phase noise testing [5], or EVM measurements [6]. Regarding test stimulus generation, many studies deal with the generation of pure sine-wave signals using digital resources [7-8]. Other works have explored the test of RF receivers based on excitation with pulse sequences [9] or

digitally-generated multi-tone signals [10] instead of the modulated signals used in the conventional test approach. Only a limited number of approaches target the generation of modulated signals using digital resources. An exploratory study has been carried out in simulation for the generation of OQPSK test stimuli, based on the exploitation of a harmonic replica of a modulated digital signal [11]. Using the same approach, the basis for a theoretical understanding has been established in [12] considering a simple modulation scheme, i.e. single-tone FM/PM. In the present paper, we extend this previous work by (i) developing an analytical expression of the modulated digital signal and defining an accurate corruption estimator that allows to identify favorable sampling conditions, (ii) providing experimental validation of the theoretical developments and (iii) demonstrating the implementation of the proposed strategy on a practical case study.

The paper is organized as follows. The principle of the digital-based strategy for the generation of modulated test stimuli is introduced in Section II. Theoretical developments are detailed in Section III and validated in Section IV. Implementation on a practical case study is discussed and demonstrated through hardware measurements in Section V. Finally, Section VI concludes the paper and presents directions for future work.

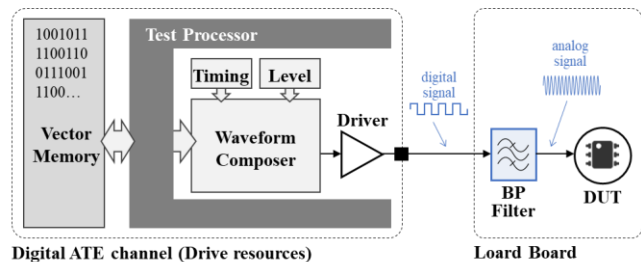
## II. DIGITAL-BASED STRATEGY FOR TEST SIGNAL GENERATION

The proposed strategy for reducing the cost of analog/RF testing is to develop new solutions that can be applied with digital test resources instead of analog/RF instruments. In particular, the objective is to enable low-cost sensitivity test of receivers, which is the classical performance measured during production test. The targeted solution is illustrated in Figure 1. It relies on the generation of a single-tone modulated test stimulus using the standard resources of a digital ATE channel.

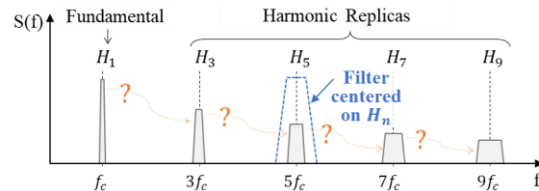
Basically, these resources involve a memory, a test processor (sequencer), a waveform composer associated with timing and level formatters and a driver. The electrical signal delivered by the driver depends on both the digital data stored in the vector memory and the programmed timing and level information. More precisely, timing information includes the definition of the tester period ( $T_{cycle}$ ), which gives the duration of one bit contained in the vector memory, as well as the specific edge locations for driving data within the tester period. The level information includes the definition of the voltage values used to drive a high level ( $V_{IH}$ ) and a low level ( $V_{IL}$ ). The test processor reads the content of the vector memory and formats it according to the programmed timing and level information. The resulting signal is then a binary signal with an amplitude  $A = (V_{IH} - V_{IL})/2$ , whose transitions occur on a sampled-time grid determined by the ATE operating frequency  $f_{ATE} = 1/T_{cycle}$ .

The binary signal generated by a standard digital tester channel (hereinafter referred to as the baseband digital signal) differs from the analog modulated test stimulus classically used for the test of RF receivers. Yet, such a digital signal can be viewed as an infinite sum of sinusoidal signals of different frequencies, amplitudes and phases. In the frequency domain, a

modulated digital signal therefore exhibits a baseband spectrum located around the signal frequency, together with harmonic replicas located around multiples of the signal frequency (odd multiples only if the digital signal has a 50% duty cycle), as illustrated in Figure 1.b. The idea is to exploit either the baseband spectrum or one of the harmonic replicas as test stimulus for the Device Under Test (DUT). In order to keep only the targeted replica, a filter can be placed on the load board that provides the interface between the ATE and the DUT, with a center frequency and bandwidth matched to the carrier frequency and bandwidth of the targeted modulated signal. Note that in many RF receivers, such a filter is already present within the DUT itself; the presence of the filter on the load board is not necessary in this case.



(a) Hardware resources



(b) Harmonic filtering of the digital signal

Fig. 1. Targeted solution for digital generation of the test stimulus.

Note that standard digital ATEs have a maximum sampling rate of 1.6GS/s. Filtering the baseband spectrum therefore restricts the solution to the generation of signals below 800MHz. This is a strong limitation, as it does not permit to address the ISM 868MHz, 915MHz, and 2.4GHz frequency bands, which are used by most RF communication devices. By exploiting harmonic replicas instead of baseband spectrum as suggested in [13], we can bypass this limitation and generate test stimuli with a frequency higher than the ATE maximum operating frequency. However; it is necessary to understand how the amplitude and the spectral content of the harmonic replicas relate to the baseband spectrum in order to encode the appropriate information in the modulated digital signal. The fact that an ATE is a sampled-time system has also to be taken into account. Both aspects are addressed in this paper, with the derivation of an analytical expression for the modulated digital signal and the definition of a corruption estimator ( $HRCE$  for Harmonic Replica Corruption Estimator) that allows the identification of non-destructive sampling conditions.

## III. THEORETICAL DEVELOPMENTS

In this section, we conduct a theoretical analysis in order to understand the properties of a modulated digital signal generated by means of a digital ATE channel, using a simple modulation scheme, i.e. single-tone FM/PM modulation.

A mathematical model which represents how the signal generated by a digital ATE channel can be derived from a conventional analog signal has been defined. As depicted in Figure 2, it involves three successive operations:

- A level discretization: Zero-Crossing (ZC),
- A time discretization: Sampling (S),
- Zero-Order Hold (ZOH).

The zero-crossing operation transforms the continuous-time analog signal into a continuous-time digital signal. The sampling process converts the continuous-time digital signal into a discrete sequence of samples; each sample directly corresponds to the binary value that will be stored in the ATE vector memory. Finally, the zero-order hold operation restores a continuous-time digital signal, but whose transitions are synchronous with the sampling clock.

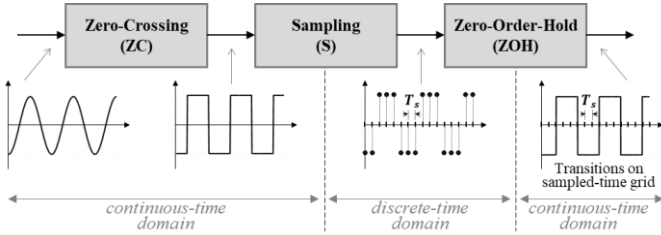


Fig.2. Mathematical model for signal generation using an ATE digital channel.

The effect of the zero-crossing operation applied on a modulated analog signal is first analyzed and an analytical expression of the continuous-time modulated digital signal is established. The effect of the sampling and zero-order hold operations is then analyzed in order to define the analytical expression of a modulated signal generated by a digital ATE channel. Finally, based on this expression, a corruption estimator is proposed which permits to identify favorable conditions for non-destructive sampling.

#### A. Effect of zero-crossing on an analog signal

Let us consider the general form of a single-tone frequency-modulated (FM) or phase-modulated (PM) signal [14]:

$$y(t) = A \cos(\Phi(t)) = A \cos(\omega_c t + \beta \sin(\omega_m t)) \quad (1)$$

where  $\Phi(t)$  is the instantaneous phase of the modulated signal,  $A$  is the amplitude of the carrier signal,  $\omega_c$  and  $\omega_m$  are the angular frequency of the carrier and message signals, and  $\beta$  is the modulation index. This expression is valid for both FM and PM signals, only the definition of the modulation index differs:  $\beta_{FM} = k_f A_m / \omega_m$  and  $\beta_{PM} = k_p A_m$ , where  $A_m$  is the message amplitude,  $k_f$  (in radians/volt-sec) and  $k_p$  (in radians/volt) being the deviation sensitivity.

By developing the cosine term of Eq.1 and using the Jacobi expansion, another expression can be obtained, involving Bessel coefficients:

$$y(t) = A \sum_{n=-\infty}^{\infty} J_n(\beta) \cos(2\pi(f_c + n f_m)t) \quad (2)$$

This expression establishes that the spectrum of a frequency or phase-modulated signal comprises a central component at the carrier frequency  $f_c$  and a series of sidebands located on both sides of the carrier frequency at  $f_c \pm n f_m$ , whose magnitudes

are determined by the Bessel coefficients  $J_n(\beta)$ .

The spectrum can significantly differ depending on the modulation index, but globally the number of sidebands that hold significant power increases (i.e. the required bandwidth to transmit the signal) as the modulation index increases. The empirical Carson's rule defines the effective transmission band  $B_T$  ( $\approx 98\%$  or more of transmitted power) with:

$$B_T = 2(\beta + 1)f_m \quad (3)$$

Let us now analyze the effect of a zero-crossing operation applied on an analog signal. First, we consider an ideal non-modulated sine-wave carrier of amplitude  $A_c$  and frequency  $f_c$ . The resulting signal is an ideal square-wave signal at the same frequency  $f_c$ . Using Fourier series expansion, this signal can be expressed as an infinite sum of sinusoids:

$$x_c(t) = \frac{4}{\pi} \left( A \cos(\omega_c t) + \frac{A}{3} \cos(3\omega_c t) + \frac{A}{5} \cos(5\omega_c t) + \dots \right) \quad (4)$$

where  $A$  is the square-wave amplitude and  $\omega_c = 2\pi f_c$ .

From this well-known expression, it can be seen that the zero-crossing operation creates harmonic tones located at odd multiples of the baseband carrier frequency, whose amplitude is reduced by the harmonic order.

In the same way, we can express a modulated digital signal as an infinite sum of modulated analog signals:

$$y(t) = \frac{4}{\pi} \left( A \cos(\Phi(t)) + \frac{A}{3} \cos(3\Phi(t)) + \frac{A}{5} \cos(5\Phi(t)) + \dots \right) \quad (5)$$

Referring to Eq.1, in case of FM/PM modulation, the instantaneous phase  $\Phi(t)$  is given by:

$$\Phi(t) = \omega_c t + \beta \sin(\omega_m t) \quad (6)$$

Inserting this expression in Eq.5, the modulated digital signal is given by:

$$y(t) = \frac{4}{\pi} \left( A \cos(\omega_c t + \beta \sin(\omega_m t)) + \frac{A}{3} \cos(3\omega_c t + 3\beta \sin(\omega_m t)) + \frac{A}{5} \cos(5\omega_c t + 5\beta \sin(\omega_m t)) + \dots \right) \quad (7)$$

which can be re-expressed as:

$$y(t) = \frac{4}{\pi} \sum_i \frac{A}{i} \cos(2\pi i f_c t + i\beta \sin(2\pi f_m t)) \text{ for } i = 1, 3, 5, \dots \quad (8)$$

This expression clearly reveals that a modulated digital signal is a sum of modulated analog signals located at odd multiples of the baseband signal, with a modification of both the amplitude and the modulation index for each individual modulated analog signal.

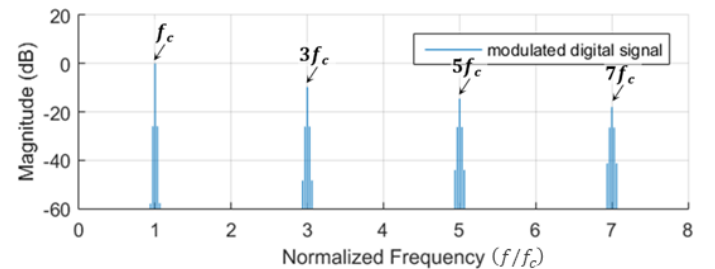


Fig.3. Spectrum of the modulated digital signal obtained from zero-crossing of a modulated analog signal.

As an illustration, Figure 3 shows the spectrum obtained from an FFT applied on a zero-crossed FM analog signal with  $f_c = 1\text{MHz}$ ,  $f_m = 30\text{kHz}$  and  $\beta = 0.1$ , the amplitude of the digital signal being set to  $A_c = \pi/4$ . As expected, the spectrum

exhibits several replicas centered on odd multiples of the carrier frequency, each replica presenting sidebands located at  $if_c \pm nf_m$ . The baseband spectrum has exactly the same characteristics than the spectrum of the original modulated analog signal, while the replicas are a transformed version of the baseband spectrum, with modification both in terms of spectral content and amplitude. For each replica, the harmonic order comes as multiplier for the modulation index and as a divider for the amplitude of the spectral components.

Going back to Eq.8 and introducing the Jacobi expansion, another expression of the modulated digital signal can be determined:

$$y(t) = \frac{4}{\pi} \sum_i \frac{A_c}{i} \left[ \sum_{n=-\infty}^{\infty} J_n(i\beta) \cos(2\pi(if_c + n f_m) t) \right] \quad \text{for } i = 1, 3, 5, \dots \quad (9)$$

Figure 4 shows the comparison between the spectrum obtained from an FFT applied on the modulated digital signal and the one derived from the values of the Bessel coefficients involved in Eq.9, with a zoom around the carrier frequency and the first two replicas. A perfect match can be observed for both the central frequency and the sidebands amplitude.

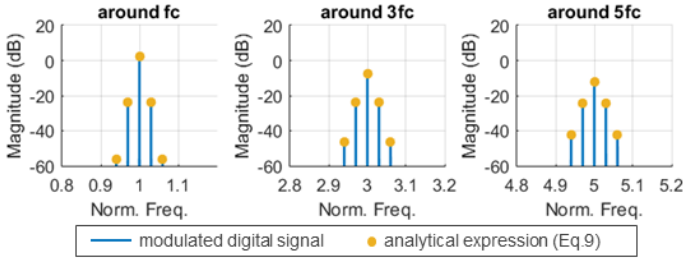


Fig.4. Zoom around the carrier frequency and the first two odd replicas.

Eq.9 is a key element of the proposed strategy because it establishes the link between the spectral content and the amplitude of a given replica and the parameters used for the modulation of the baseband digital signal. It therefore permits to choose appropriate settings of the baseband signal to reach desired characteristics around a given replica. Practically, to obtain a modulated signal with carrier frequency  $f_{c_{target}}$ , carrier amplitude  $A_{c_{target}}$  and modulation index  $\beta_{target}$ , the baseband digital signal should be generated with  $f_c = f_{c_{target}}/i$ ,  $A_c = \pi i A_{c_{target}}/4$  and  $\beta = \beta_{target}/i$ , where  $i$  is the order of the selected harmonic replica.

### B. Effect of sample-and-hold on a digital signal

Sampling is the process of converting a continuous-time signal into a discrete sequence of samples. Mathematically, the sampled signal can be expressed as the multiplication of the analog signal  $x(t)$  by a Dirac comb  $\text{III}_{T_s}(t)$ :

$$x_s(t) = x(t) * \text{III}_{T_s}(t) = x(t) * \sum_{k=-\infty}^{+\infty} \delta(t - kT_s) \quad (10)$$

Taking the Fourier transform, the expression in the frequency domain is given by:

$$X_s(f) = X(f) \otimes \frac{1}{T_s} \text{III}_{f_s}(f) = \frac{1}{T_s} \sum_{k=-\infty}^{+\infty} X(f - kf_s) \quad (11)$$

As indicated by Eq.11, sampling induces a periodization of the spectrum, with copies of the original spectrum (called images) shifted by multiples of the sampling frequency and summed. This expression is the basis of the Nyquist theorem that states that a band-limited signal can be fully represented if sampled at a frequency  $f_s$  which is greater than twice the maximum frequency component  $f_M$  in the signal:  $f_s > 2 * f_M$ . Indeed, when this criterion is satisfied, there is no overlap between the baseband spectrum and the images created by the sampling process. An extension of the Nyquist theorem concerns narrowband signals, i.e. signals that have a limited bandwidth around a given frequency and that do not extent to DC. In this case, it is possible to sample the signal below the Nyquist rate while still obtaining a perfect signal representation in the Nyquist band, upon specific conditions on the sampling frequency. Such process is called undersampling, harmonic sampling or bandpass sampling.

In our context, the modulated digital signal obtained from zero-crossing has theoretically an infinite number of replicas, so an infinite bandwidth. However, each replica is a narrow-band signal. So, depending on the value of the sampling frequency, some replicas will satisfy the Nyquist criterion while others will be undersampled.

Moreover, the signal generated by the digital ATE channel corresponds to a zero-order held version of the sampled signal. Mathematically, this is expressed by a convolution between the sampled signal  $x_s(t)$  and a rectangular function  $\Pi_{T_s}\left(t - \frac{T_s}{2}\right)$ , where  $T_s$  is the sampling period:

$$x_{s-ZOH}(t) = x_s(t) \otimes \Pi_{T_s}\left(t - \frac{T_s}{2}\right) = [x(t) * \text{III}_{T_s}(t)] \otimes \Pi_{T_s}\left(t - \frac{T_s}{2}\right) \quad (12)$$

Taking the Fourier transform, the expression in the frequency domain is given by:

$$X_{s-ZOH}(f) = \left[ \frac{1}{T_s} \sum_{k=-\infty}^{+\infty} X(f - kf_s) \right] * T_s * \text{sinc}(\pi T_s f) * e^{-i\pi T_s f} = \text{sinc}(\pi T_s f) * e^{-i\pi T_s f} \sum_{k=-\infty}^{+\infty} X(f - kf_s) \quad (13)$$

The zero-order hold process therefore introduces a global shaping of the periodized spectrum by the  $\text{sinc}$  function.

#### 1) Non-modulated signal

Let us first investigate the effects of the sample-and-hold operations on a non-modulated digital signal, i.e. a simple square-wave signal. For the following analysis, the ratio between the sampling frequency and the signal one is defined as the Number of Samples Per Period  $NSPP = f_s/f_c$ . Figure 5 shows the spectrum of the sampled-and-held signal for an arbitrary value of  $NSPP = 6.3$ . The expected harmonic tones at odd multiples of the signal frequency are present but they are mixed with other components of similar or even higher amplitude. The components of high amplitude actually correspond to high-frequency images of the harmonic tones located below the Nyquist frequency, while the other additional components correspond to low-frequency images of the harmonic tones located above the Nyquist frequency (harmonic

tones of order superior or equal to 5 for this example). Because on this example the  $NSPP$  is a non-integer value, these images do not necessarily fall at odd multiples of the signal frequency; they are actually located at multiples of  $0.1 * f_c$ . The global shaping of the spectrum by the  $\text{sin}_c$  function which has local zeros at every multiple of the sampling frequency is also clearly observed; all components close to these local zeros are cancelled. In the context of the proposed strategy, care must be taken to ensure that useful information does not fall close to these local zeros. In particular, the sampling frequency must not be (and preferably not close to) a sub-multiple or multiple of the targeted replica frequency.

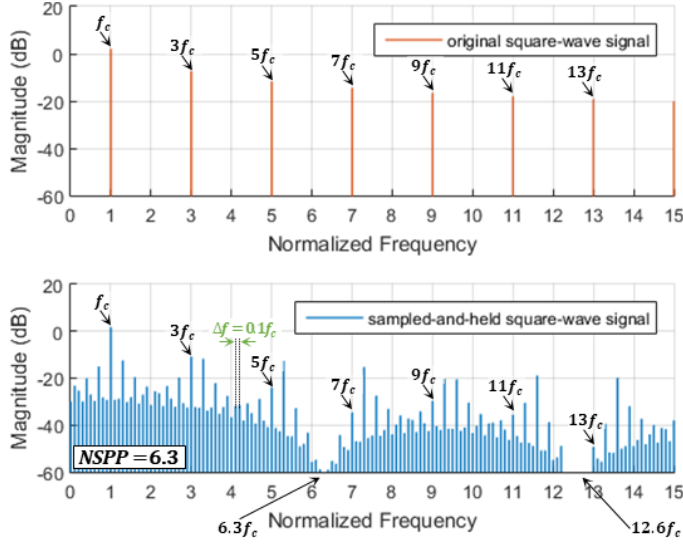


Fig.5. Spectrum comparison between original square-wave signal and sampled-and-held signal with  $NSPP = 6.3$ .

Our objective is to establish an analytical expression of the sampled-and-held signal spectrum so that we can easily investigate the transformations brought on the original spectrum depending on the  $NSPP$  value. Referring to the general theory, we can express the sampled-and-held signal as a square-wave signal multiplied by a Dirac comb  $\text{III}_{T_s}(t)$  (sampling operation), which is convoluted with a rectangular function  $\Pi_{T_s}\left(t - \frac{T_s}{2}\right)$  (hold operation).

For the sake of simplicity, we consider a shifted and scaled version of the square-wave signal whose amplitude varies between 0 and 1 (the actual square-wave signal has an amplitude that varies between  $+A$  and  $-A$ ), which can be modeled by a convolution product between a rectangular function  $\Pi_{T/2}(t)$  and a Dirac comb  $\text{III}_T(t)$ :

$$x_c(t) = \Pi_{T/2}(t) \otimes \text{III}_T(t) \quad (14)$$

where  $T = 1/f_c$  is the period of the square-wave signal.

The sampled-and-held signal can therefore be expressed by:

$$\tilde{x}_c(t) = \left[ \left( \Pi_{T/2}(t) \otimes \text{III}_T(t) \right) * \text{III}_{T_s}(t) \right] \otimes \Pi_{T_s}\left(t - \frac{T_s}{2}\right) \quad (15)$$

Using the Fourier transform, the signal in the frequency domain is:

$$\tilde{X}_c(f) = \left[ \left( \frac{T}{2} * \text{sin}_c\left(\frac{\pi T f}{2}\right) * \frac{1}{T} \text{III}_{f_c}(f) \right) \otimes \frac{1}{T_s} \text{III}_{f_s}(f) \right] * T_s * \text{sin}_c(\pi T_s f) * e^{-i\pi T_s f} \quad (16)$$

Then:

$$\tilde{X}_c(f) = \left[ \left( \frac{1}{2} \text{sin}_c\left(\frac{\pi T f}{2}\right) \sum_{k=-\infty}^{+\infty} \delta(f - k f_c) \right) \otimes \sum_{l=-\infty}^{+\infty} \delta(f - l f_s) \right] * \text{sin}_c(\pi T_s f) * e^{-i\pi T_s f} \quad (17)$$

After manipulation and simplification, it comes:

$$\tilde{X}_c(f) = \frac{1}{2} e^{-i\pi T_s f} \sum_{k=-\infty}^{+\infty} \sum_{l=-\infty}^{+\infty} \text{sin}_c\left(\frac{\pi k}{2}\right) * \text{sin}_c\left(\pi \left(k \frac{T_s}{T} + l\right)\right) * \delta(f - (k f_c + l f_s)) \quad (18)$$

By using the greatest common divisor between the signal frequency and the sampling frequency  $\Delta f = \text{gcd}(f_c, f_s)$ , we can re-express the term in the Dirac function:

$$k f_c + l f_s = (kx + ly)\Delta f \quad \text{with } x = f_c/\Delta f \text{ and } y = f_s/\Delta f \quad (19)$$

Introducing this form in Eq.18, the final expression of the sampled-and-held signal is:

$$\tilde{X}_c(f) = \frac{1}{2} e^{-i\pi T_s f} \sum_{k=-\infty}^{+\infty} \sum_{l=-\infty}^{+\infty} A_{k,l} \delta(f - (kx + ly)\Delta f) \quad (20)$$

$$\text{with } A_{k,l} = \text{sin}_c\left(\frac{\pi k}{2}\right) * \text{sin}_c\left(\pi \left(\frac{k}{NSPP} + l\right)\right)$$

This expression clearly establishes that the spectrum of the sampled-and-held square-wave signal exhibits frequency components located at multiples of  $\Delta f$ , whose amplitude depends on the  $NSPP$  value.

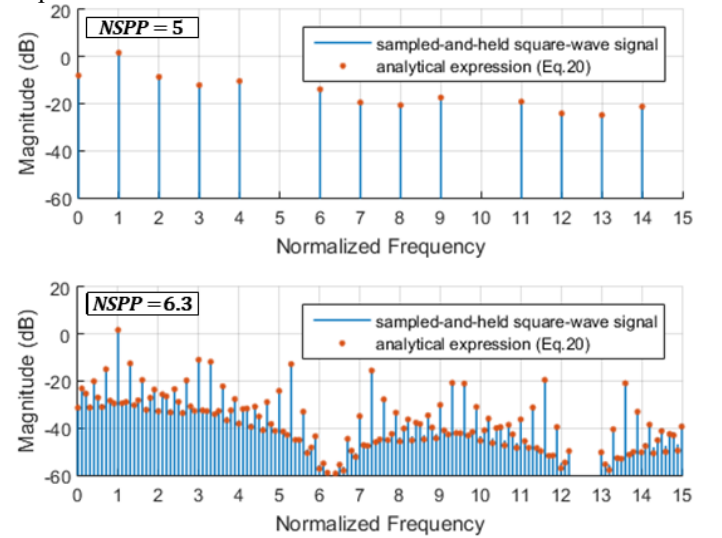


Fig.6. Comparison between the spectrum obtained from an FFT on the sampled-and-held square-wave signal and the one derived from the analytical expression.

Figure 6 shows the comparison between the spectrum computed with an FFT applied on the continuous-time digital signal obtained after sample and hold operations and the one computed with Eq.20 (a factor  $2A$  has been applied on the amplitude to take into account a symmetrical square-wave signal with an amplitude that varies between  $+A$  and  $-A$ ), for an integer and a non-integer value of  $NSPP$ . In both cases, a perfect match can be observed both on the amplitude and the location of the spectral components. Note that in case of an integer  $NSPP$  value,  $\Delta f = \text{gcd}(f_c, f_s) = f_c$ , which means that all the images of the harmonic tones fall at multiples of the baseband signal frequency  $f_c$ . The amplitude at a given multiple of the baseband signal frequency therefore corresponds to the

sum of the original tone plus the contribution of all the folded images. Note also that even harmonics appear in case of odd  $NSPP$  value, due to folded components that fall at even multiples of the baseband signal frequency. In case of a rational  $NSPP$  value, only a limited number of folded images fall at multiples of the baseband signal frequency and might bring only a negligible contribution compared to the original tone. This is specifically the case with the chosen  $NSPP = 6.3$ , where components are spread all over multiples of  $\Delta f = 0.1f_c$ .

## 2) Modulated signal

Now, let us analyze the effects of the sample-and-hold operations on a modulated digital signal with  $f_c = 1\text{MHz}$ ,  $f_m = 30\text{kHz}$  and  $\beta = 0.1$ . As in the case of a simple square-wave signal, we expect that the harmonic replicas that contain the modulation sidebands will be present in the spectrum, but mixed with additional components created by the sampling process. The shaping by the  $\text{sinc}$  function will also apply, which means that the amplitude of the spectral components will be affected. In particular, assuming that there is no overlap between a given harmonic replica and images of other replicas, the expected amplitude of the central and sideband components is given by:

$$A_{i,n}^{\text{expected}} = A * \frac{4J_{|n|}(i\beta)}{\pi i} * \text{sinc}\left(\frac{\pi i}{NSPP}\right) \quad \text{for } i = 1, 3, 5, \dots \quad (21)$$

where  $i$  is the order of the replica and  $n$  the order of the sideband components located at  $if_c \pm nf_m$  ( $n = 0$  for the central component located at  $if_c$ ).

Figure 7 illustrates the spectrum of the sampled-and-held modulated digital signal for different  $NSPP$  values; the expected amplitude if no overlap is also plotted (dot markers). Several comments arise from this figure. First regarding the case of integer  $NSPP$ , harmonic replicas are observed at odd multiples of the carrier frequency when using  $NSPP = 16$ . However, the amplitude of the central and sideband components do not match with the expected one. Indeed in this case, images created by the sampling process are superimposed onto the existing replicas of the original signal. Since the modulation index changes with the replica order, the spectral content of the original replicas is modified and no longer corresponds to the expected one. In case of  $NSPP = 6$ , only a single frequency component is observed at odd multiples of the carrier frequency. Indeed, when the  $NSPP$  is not sufficiently high, the sampling process does not permit to capture the modulation effect (i.e. change in the instantaneous frequency) and simply converts the modulated square-wave into a non-modulated one. In the context of our strategy, both these situations should be avoided, which means that the sampling frequency must not be a multiple of the carrier frequency. Finally in case of  $NSPP = 6.3$ , the overall spectrum appears rather misted but the expected harmonic replicas are clearly visible and the amplitudes of the central and the first sidebands components are in good agreement with those expected, as illustrated by the close-up view around the carrier frequency and the first two odd replicas given in Figure 8. As in the case of the non-modulated signal, we note the presence of low-amplitude additional components, located here at multiples of

$0.01 * f_c$ . This example illustrates that despite all the modifications brought by the sample-and-hold process, it is possible to preserve the spectral content related to the modulation around the harmonic replicas, provided a pertinent choice of  $NSPP$ .

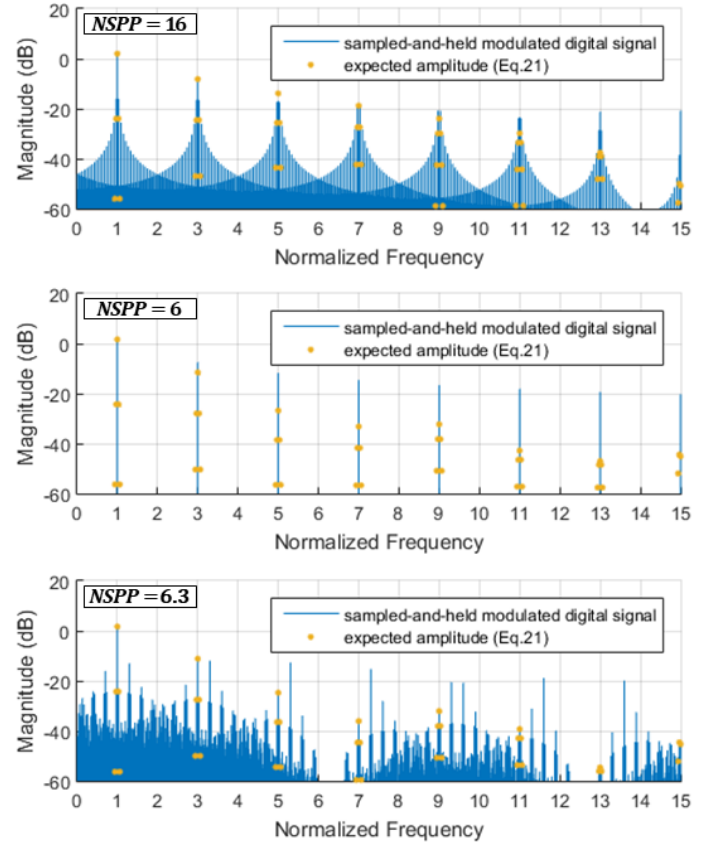


Fig.7. Spectrum comparison between original modulated digital signal and sampled-and-held signal for different  $NSPP$  values.

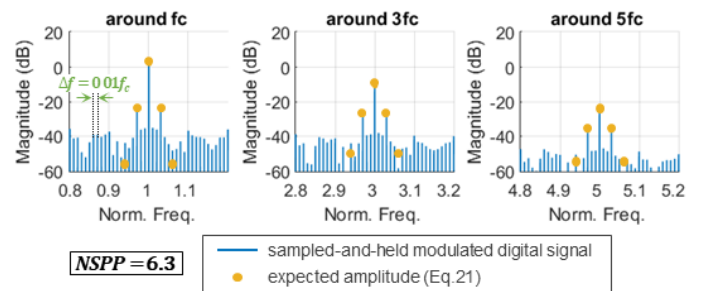


Fig.8. Zoom around the carrier frequency and the first two odd replicas of the sampled-and-held modulated digital signal with  $NSPP = 6.3$ .

In order to derive an analytical expression of the sampled-and-held modulated digital signal, we start again with the basic equation that states that a sampled-and-held signal corresponds to the original modulated digital signal  $y(t)$  multiplied by a Dirac comb  $\text{III}_{T_s}(t)$ , and convoluted with a rectangular function  $\Pi_{T_s}\left(t - \frac{T_s}{2}\right)$ :

$$\tilde{y}(t) = [y(t) * \text{III}_{T_s}(t)] \otimes \Pi_{T_s}\left(t - \frac{T_s}{2}\right) \quad (22)$$

Introducing the expression of the original modulated digital signal  $y(t)$  established in section III.A. (Eq.9), and taking the Fourier transform, it comes:

$$\tilde{Y}(f) = \left[ \left( \sum_i \sum_{n=-\infty}^{\infty} \frac{4AJ_n(i\beta)}{\pi i} * \frac{1}{2} (\delta(f - if_c - nfm) + \delta(f + if_c - nfm)) \right) \otimes \frac{1}{T_s} \text{III}_{f_s}(f) \right] * T_s * \text{sin}_c(\pi T_s f) * e^{-i\pi T_s f} \quad (23)$$

After some mathematical manipulations, we obtain:

$$\tilde{Y}(f) = e^{-i\pi T_s f} \sum_{p=-\infty}^{+\infty} \sum_{n=-\infty}^{+\infty} \sum_{q=-\infty}^{+\infty} \frac{4AJ_n((2p+1)\beta)}{\pi(2p+1)} * \text{sin}_c \left( \pi \left( (2p+1) \frac{f_c}{f_s} + n \frac{f_m}{f_s} + q \right) \right) * \delta \left( f - ((2p+1)f_c + n f_m + q f_s) \right) \quad (24)$$

This signal exhibits frequency components located at multiples of  $\Delta f_{mod}$ , where  $\Delta f_{mod}$  is given by the greatest common divisor between the carrier frequency  $f_c$ , the message frequency  $f_m$  and the sampling frequency  $f_s$ :

$$\Delta f_{mod} = \text{gcd}(f_c, f_m, f_s) \quad (25)$$

Using  $x = f_c/\Delta f_{mod}$ ,  $y = f_m/\Delta f_{mod}$  and  $z = f_s/\Delta f_{mod}$ , the final expression of the sampled-and-held modulated digital signal is:

$$\tilde{Y}(f) = e^{-i\pi T_s f} \sum_{p=-\infty}^{+\infty} \sum_{n=-\infty}^{+\infty} \sum_{q=-\infty}^{+\infty} A_{p,n,q} * \delta(f - ((2p+1)x + ny + qz)\Delta f_{mod}) \quad (26)$$

$$\text{with } A_{p,n,q} = A * \frac{4J_n((2p+1)\beta)}{\pi(2p+1)} * \text{sin}_c \left( \pi \left( \frac{2p+1}{NSPP} + \frac{n f_m}{NSPP * f_c} + q \right) \right)$$

This expression establishes that the spectrum of the sampled-and-held modulated digital signal has frequency components located at multiples of  $\Delta f_{mod}$ , (explaining components located at multiples of  $0.01 * f_c$ . in Figure 8), whose amplitude depends on the Bessel coefficients and the  $NSPP$  value.

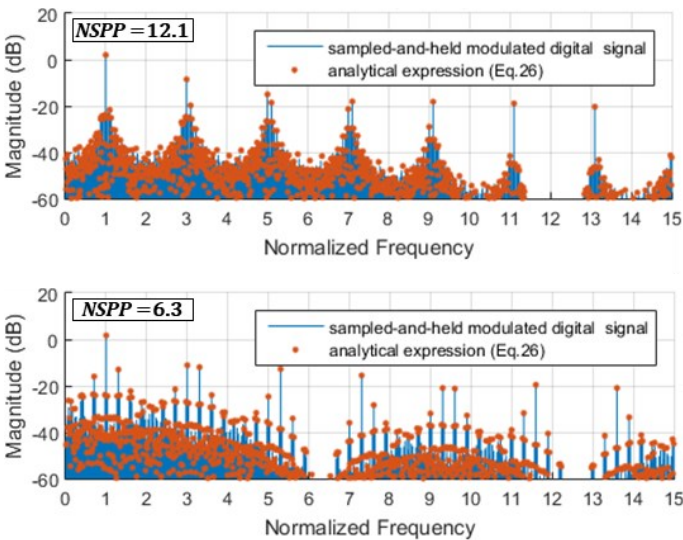


Fig.9. Comparison between the spectrum obtained from an FFT on the sampled-and-held modulated digital signal and the one derived from the analytical expression.

As an illustration, Figure 9 shows the comparison between the spectrum obtained from an FFT applied on time-domain signal and the one computed with Eq.26 for two different cases of  $NSPP$  values. A good agreement on the amplitude and the location of the most significant components is observed.

### C. Conditions for non-destructive sampling

The main challenge is now to easily identify the values of the sampling frequency that allow non-destructive sampling for a given harmonic replica, i.e. no overlap between the targeted replica and images of other replicas with significant magnitude. The problem is highly complex, and all our attempts to derive a formal equation that expresses this condition have been unsuccessful so far. However, the analytical expressions developed in the previous section give us the opportunity of defining an estimator representative of the corruption around a given harmonic replica. A first estimator was defined in [12], based on the analytical expression of the sampled-and-held digital carrier (Eq.20). In this paper, we proposed a more refined estimator based on the analytical expression of the sampled-and-held modulated digital signal. This estimator relies on three performance metrics illustrated in Figure 10 and detailed hereafter.

- $HCP_i$ : the Harmonic Carrier Power of a replica  $i$  is defined as the power contained in its central frequency component:

$$HCP_i = H_i^2 \quad (27)$$

The expected value of the Harmonic Carrier Power can be defined from Eq.21 with:

$$\begin{aligned} HCP_i^{expected} &= (A_{i,0}^{expected})^2 \\ &= \left( \frac{4AJ_0(i\beta)}{\pi i} * \text{sin}_c \left( \frac{\pi i}{NSPP} \right) \right)^2 \end{aligned} \quad (28)$$

A deviation from the expected value is representative of images that strongly interact with the considered replica. In this case, control of the amplitude of the harmonic replica by adjusting the amplitude  $A$  of the signal delivered by the ATE is no longer guaranteed.

- $HSBP_i$ : the Harmonic Sidebands Power of a replica  $i$  is defined as the power contained in the sideband components comprised in the bandwidth  $B_{T_i}$ :

$$HSBP_i = \sum_{n \geq 1} SB_{i,n}^2 + SB_{i,-n}^2 \quad (29)$$

The expected value of the Harmonic Sidebands Power is characteristic of the modulation index value and can be derived from the Bessel coefficients taking into account the  $\text{sin}_c$  shaping:

$$\begin{aligned} HSBP_i^{expected} &= \sum_{n \geq 1} (2 * A_{i,n}^{expected})^2 \\ &= \frac{4A}{\pi i} * \text{sin}_c \left( \frac{\pi i}{NSPP} \right) \sum_{n \geq 1} (2 * J_n(i\beta))^2 \end{aligned} \quad (30)$$

A deviation from the expected value is representative of an overlap between the sideband components of the targeted replica and images of other replicas. In this case, the spectral content related to the modulation will be altered.

- $HDP_i$ : the Harmonic Distortion Power of a replica  $i$  is

defined as the power contained in all the spectral components comprised within an enlarged bandwidth  $\alpha B_{T_i}$ , except the central frequency and sideband components:

$$HDP_i = \sum_{m \geq 1} D_{i,m}^2 + D_{i,-m}^2 \quad (31)$$

where  $\alpha$  is a factor higher than 1 that permits to choose to size of the enlarged bandwidth. For the following experiments, we arbitrarily choose  $\alpha = 3$ . In a practical situation, this factor should be chosen in accordance with the selectivity of the bandpass filter placed on the load board.

In ideal conditions, no image of harmonic replicas should be present in the signal bandwidth nor in its close vicinity; the expected value of the Harmonic Distortion Power in the enlarged bandwidth is therefore zero. Any deviation from zero is representative of the presence of an unwanted component in the region of interest.

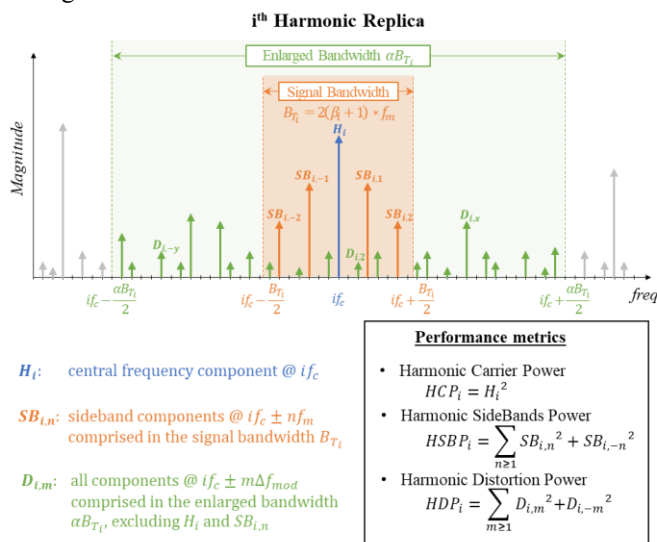


Fig.10. Definition of performance metrics for a given harmonic replica.

Based on these three metrics, we can define a global estimator that expresses the overall corruption of a given replica with:

$$HRCE_i = \frac{|HCP_i - HCP_i^{expected}| + |HSBP_i - HSBP_i^{expected}| + HDP_i}{HCP_i^{expected}} \quad (32)$$

where  $HRCE$  stands for Harmonic Replica Corruption Estimator.

The numerator term is representative of the deviation of both the carrier and sidebands power from their expected value as well as the presence of distortion components in the bandwidth and in its vicinity. The denominator term acts as a penalty factor to account for the reduced amplitude as the replica order increases and the global  $\sin_c$  shaping induced by the hold process. In particular, the closer the replica  $i$  is from a local zero of the  $\sin_c$  function, the higher the penalty factor. Indeed, the proximity of a replica with a local zero entails a strong attenuation that might compromise baseband signal generation with sufficient amplitude. It also involves a dissymmetry between positive and negative sidebands that alters the spectral content related to the modulation. This estimator permits to

have a quantitative evaluation of the quality of the signal generated by the ATE around a given harmonic replica, for any potential sampling frequency. The closer this estimator is to zero, the better the quality of the generated signal.

Practically,  $HCP_i$ ,  $HSBP_i$  and  $HDP_i$  metrics are evaluated from  $\tilde{Y}(f)$  defined by Eq.26 using only a limited number of combinations ( $|p| < 30$ ),  $|n| \leq 10$  and  $|q| < 30$ ). Frequency components that fall within the interval  $\left[ f_c - \frac{\alpha B_{T_i}}{2}, f_c + \frac{\alpha B_{T_i}}{2} \right]$  are considered for the computation of the performance metrics.

To illustrate the usefulness of the corruption estimator, let us consider that the targeted modulated signal will be generated using the 5<sup>th</sup>-order harmonic replica, leading to  $\beta = 0.5$  which is a modulation index value typically used in real case applications. Figure 11 shows values of the corruption estimator  $HRCE_5$  computed for different values of  $NSPP$  varied between 2 and 16 by step of 0.1.

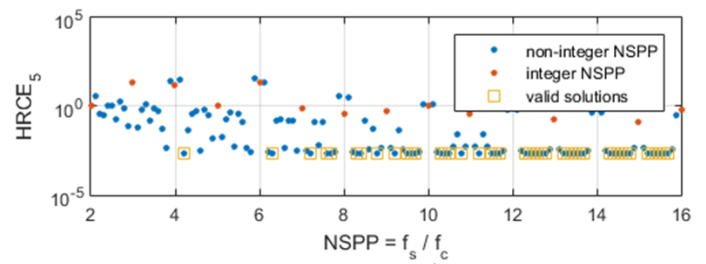


Fig.11. Corruption estimator vs.  $NSPP$  for the 5<sup>th</sup>-order harmonic replica.

Two main comments can be drawn from these results. First and as previously established, it is clear that the choice of an integer  $NSPP$  is not a favorable condition. Second, it exists a number of low-corruption solutions (highlighted with square markers), including low  $NSPP$  values. This is of foremost importance since these values are the ones that impose the least constraints on the equipment sampling capabilities.

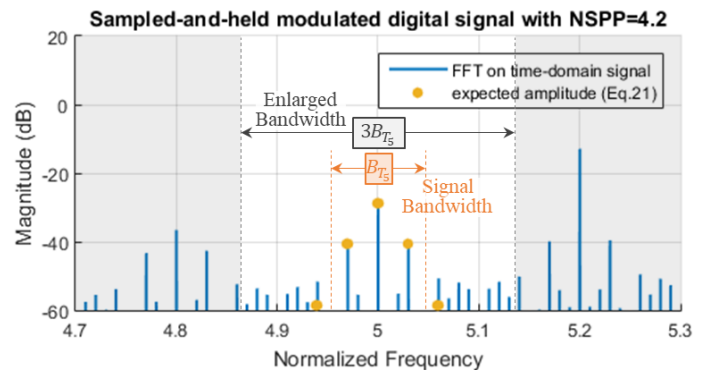


Fig.12. Spectrum of the sampled-and-held modulated digital signal with  $NSPP = 4.2$  – Zoom around the 5<sup>th</sup> harmonic replica.

For this case study, the smallest  $NSPP$  value that gives low corruption is  $NSPP = 4.2$ ; this choice is therefore a priori a favorable condition to generate a good quality signal. Figure 12 shows the spectrum obtained around the 5<sup>th</sup> harmonic. It can be observed that the central frequency and sideband components contained in the signal bandwidth are in good agreement with the expected values. The spectral content related to the modulation is therefore preserved. Moreover, the additional components contained in the signal bandwidth have an

amplitude significantly lower than the one of the central frequency and sideband components. In the same way, all components contained in the enlarged bandwidth have an amplitude significantly lower than the one of the central frequency and sideband components. Note that it exists other components with significant amplitude but they are outside the enlarged bandwidth; it is the role of the bandpass filter placed on the load board to eliminate these components. This example illustrated how the proposed corruption estimator permits to identify favorable sampling conditions.

Note that, in practice, the solution chosen will not necessarily be the one with the lowest  $NSPP$  value. In fact, the chosen solution can be any of the valid solutions below the  $NSPP$  value that complies with the equipment sampling capabilities. All these solutions are a priori equivalent in terms of spectral content. However, they may differ in terms of attenuation brought on the baseband signal, which can be calculated with:

$$Att_i = \frac{1}{\frac{4J_0(i\beta)}{\pi i} * \sin_c\left(\frac{\pi i}{NSPP}\right)} \quad (33)$$

The attenuation factor can be used as a second selection criterion, since the lower the attenuation, the more relaxed the requirement on the voltage capabilities of the test equipment.

Figure 13 shows the evolution of the attenuation factor with respect to the  $NSPP$ , for the considered example. Extremely high attenuation is observed for  $NSPP$  values close to 2.5 and 5, which correspond to situations where a local zero of the  $\sin_c$  function falls close to the 5<sup>th</sup>-order harmonic replica (sampling frequency equal to the frequency of the targeted harmonic replica or a submultiple); no valid solutions are identified in these areas. Valid solutions for this example have an attenuation factor ranging from 13.9dB and 28.8dB, with a reduction of the attenuation factor as the  $NSPP$  value increases. The best solution will therefore be determined by the highest  $NSPP$  value that can be implemented on the test equipment.

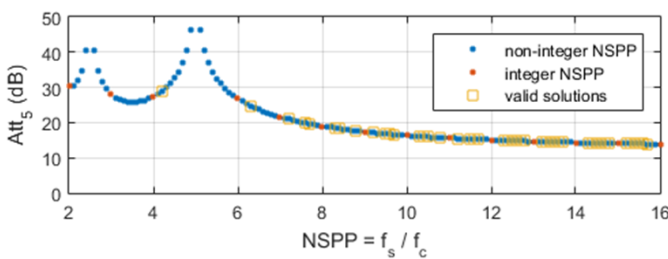


Fig.13. Attenuation factor vs.  $NSPP$  for the 5<sup>th</sup>-order harmonic replica.

#### IV. VALIDATION

##### A. Experimental setup

A test bench corresponding to the mathematical model defined in Figure 2 was implemented in order to emulate a digital ATE channel. As illustrated in Figure 14, it comprises an RF signal generator, a latched comparator, a DC power supply, a pulse generator, and a digital storage oscilloscope. The RF signal generator delivers a continuous-time modulated sine-wave signal  $y(t)$ . The generator allows to adjust the carrier amplitude  $A_c$ , the carrier frequency  $f_c$ , the message frequency  $f_m$  (message amplitude  $A_m$  is automatically set to 1) and the

maximal frequency deviation  $f_\Delta$  which controls the modulation index  $\beta = f_\Delta/f_m$ . This modulated sine-wave signal is sent to one input of the comparator; the other input of the comparator being connected to the DC power supply which delivers the threshold voltage used for the zero-crossing operation (threshold voltage should be adjusted to the mean amplitude of the generated signal). The sample-and-hold operation is performed using the latch enable input of the comparator, which is connected to the pulse generator that delivers a pulse sequence at a chosen  $f_s$  rate. The signal at the output of the comparator therefore corresponds to the sampled-and-held modulated digital signal  $\hat{y}(t)$ , i.e. the signal that would be delivered by a digital ATE channel. Acquisition of this signal is performed by the oscilloscope at 3.125Gbps and captured data are transferred to a PC for further processing (FFT).

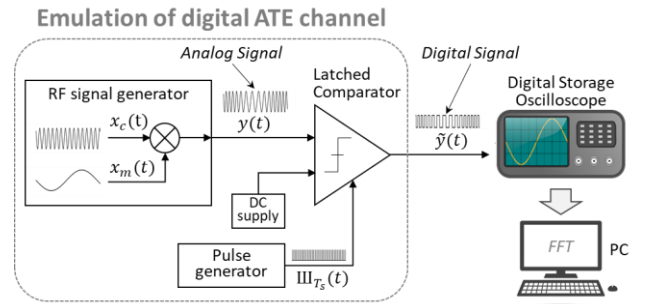


Fig.14. Experimental setup for lab experiments.

A limitation of this setup is that the digital signal amplitude cannot be freely adjusted. It is fixed by the comparator output levels, measured at  $V_H \cong 1.656 V$  for the high state and  $V_L \cong 1.280 V$  for the low state. The generated digital signal has therefore an amplitude  $A \cong 188 mV$  with a mean value of 1.468 V. The generated signal is also susceptible to be impacted by jitter or phase noise of the various clock sources. Despite these limitations, the purpose of this setup is to validate the theoretical developments presented in the paper. In practice, the digital signal will be generated by reading a sequence of binary data stored in the ATE memory, and no analog instruments will be involved.

##### B. Validation of theoretical developments

Hardware measurements were performed to corroborate the effects identified by the simulation and the theoretical analysis, considering the same case study, i.e. a modulated signal with a carrier at  $f_c = 1MHz$ , a message at  $f_m = 30kHz$  and a modulation index  $\beta = 0.1$  (frequency deviation  $f_\Delta$  set at 3kHz on the RF signal generator).

##### 1) Effect of zero-crossing on analog signals

For the first experiment, the sampling frequency was set as high as possible with  $f_s = 250MHz$ . The aim is to validate the effect of the 1-bit quantization process, independently of the effect of the sample-and-hold operations. With 250 samples per signal period, the digital signal delivered at the output of the comparator can be considered as equivalent to a signal submitted to a pure analog zero-crossing operation.

Figure 15 shows the spectrum computed on the captured transient data and compare it to that computed on a simulated

signal submitted to a zero-crossing operation (levels of the signal after zero-crossing have been set to the same values than the measured comparator output levels). Globally, the spectrum of the experimental digital signal shows a good agreement with the expected one: the main harmonic replicas are located at odd multiples of the signal frequency and exhibit decreasing amplitude and increasing modulation index as the replica order gets higher. However, the presence of small harmonic tones located at even multiples of the signal frequency can be observed. These unwanted harmonic tones come from an inaccurate adjustment of the comparator threshold to the mean amplitude of sine-wave signal delivered by the RF generator, due to the limited resolution of the DC power supply. Still, the amplitude of these unwanted tones remains much lower than the amplitude of the odd harmonic tones. The imperfect setting of the comparator threshold voltage has been included in the simulation for all the following graphs.

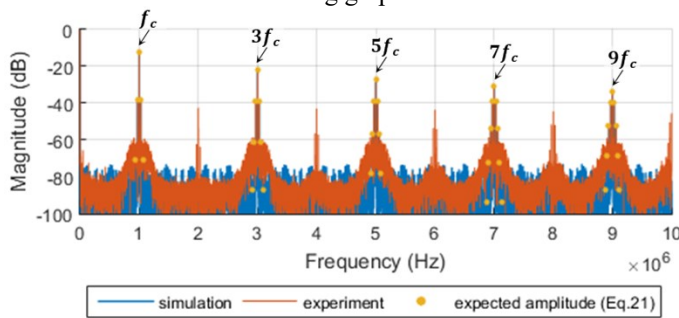


Fig.15. Effect of zero-crossing on a modulated analog signal: hardware experiment vs. simulation/theory.

To better illustrate the spectral characteristics related to the modulation, Figure 16 gives a close-view around the carrier frequency and the first two odd replicas; expected amplitudes computed by Eq.21 are also reported. The increase in the modulation index as the replica order gets higher is clearly visible, with an increase in the number of sidebands that hold significant power. It can also be seen that the amplitudes of the central frequency and significant sideband components of the experimental signal perfectly match with the expected ones.

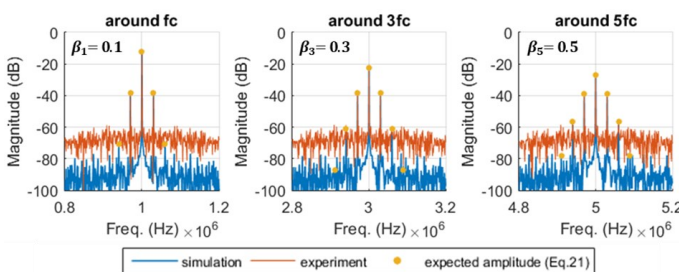


Fig.16. Effect of zero-crossing on a modulated analog signal: close-view around the carrier frequency and the first two odd replicas.

## 2) Effect of sample-and-hold on digital signals

For the following experiments, the sampling frequency was limited to less than  $20\text{MHz}$  in order to examine the effect of the sample-and-hold process on the digital signal delivered at the output of the latched comparator. Several acquisitions were carried out using different values of the sampling frequency, corresponding to the various  $NSPP$  situations investigated in the previous section. For the sake of brevity, only the results

corresponding to  $NSPP = 6$  (integer value) and  $NSPP = 4.2$  (valid solution with the lowest  $NSPP$  value) are commented.

Note that in practice, the sampling frequency cannot be set exactly to the target value due to pulse generator imprecision. For instance, when setting the sampling frequency to  $6\text{MHz}$  on the pulse generator, the measured value on the oscilloscope is  $6.007\text{MHz}$ . For proper comparison with experiments, the sampling frequency used in simulation and analytical expressions is the actual value measured on the oscilloscope. A rms jitter of  $5\text{ns}$  is also included in all simulations to verify the robustness of the proposed solution to the presence of jitter in the sampling frequency.

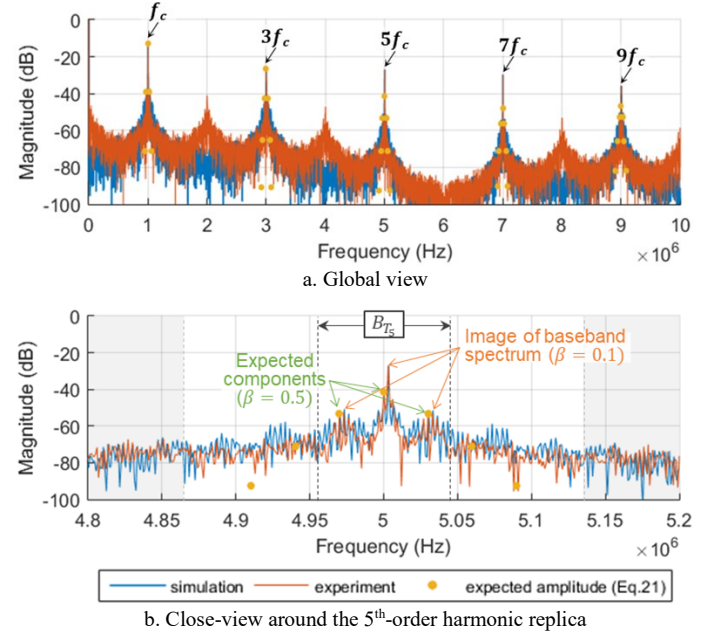


Fig.17. Effect of sample-and-hold with  $NSPP \cong 6$  on a modulated digital signal: hardware experiment vs. simulation/theory.

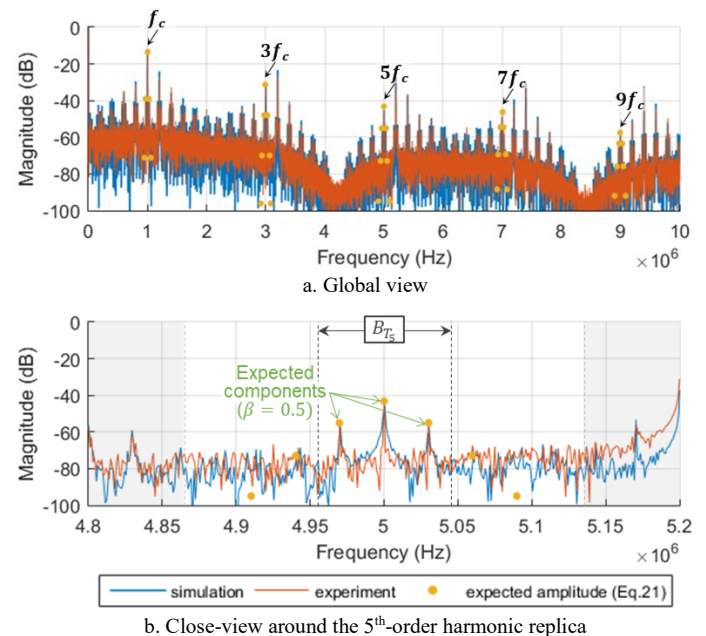


Fig.18. Effect of sample-and-hold with  $NSPP \cong 4.2$  on a modulated digital signal: hardware experiment vs. simulation/theory.

Comparison between the spectrum computed on the captured transient data and the one computed in simulation is reported in Figures 17 and 18, for  $NSPP \cong 6$  and  $NSPP \cong 4.2$  respectively. A first comment is that there is a good agreement between the experimental spectrum and the simulated one in both cases. Yet, different situations are observed depending on the  $NSPP$  value. In the case of  $NSPP \cong 6$ , the global spectrum has a clean appearance but the close-up view around the 5<sup>th</sup>-order harmonic replica reveals that the expected characteristics corresponding to a modulation index  $\beta = 0.5$  are indeed present, but they are altered by the presence of a first-order image of the baseband spectrum, which exhibits a modulation index  $\beta = 0.1$ . In contrast, in the case of  $NSPP \cong 4.2$ , the global spectrum appears hazy but the close-up view around the 5<sup>th</sup>-order harmonic replica reveals a clean spectrum with the desired modulation characteristics.

Overall, these hardware measurements corroborate the effects identified by the simulation and the theoretical analysis, and thus validate the feasibility of the proposed solution.

## V. PRACTICAL CASE STUDY

In this section, we demonstrate the implementation of the proposed solution on a practical case study. Specifically, the aim is to generate an analog modulated signal with a carrier frequency at  $f_{ctarget} = 868MHz$ , a message frequency at  $f_m = 0.75MHz$  and an effective transmission band  $B_{Ttarget} = 2.48MHz$ . This signal has to be generated from a digital signal at lower frequency, taking into account the frequency capabilities of the equipment. To illustrate the adaptability of the proposed solution, experiments are conducted assuming different constraints on the equipment, with an upper limit of the sampling frequency  $f_{smax}$  set at  $400MHz$ ,  $330MHz$  and  $240MHz$ . The high-frequency analog signal will be obtained by filtering one of the harmonic replicas of the low-frequency digital signal. The lower the limit of the sampling frequency, the more challenging the implementation of the solution.

### A. Setting of sampling frequency and baseband signal parameters

The first step is to determine the minimum order of the harmonic replica that permits to ensure that the baseband signal complies with the Nyquist criterion, taking into account the maximum sampling frequency allowed by the equipment. Considering, in first approximation, that the sampling frequency has to be higher than twice the carrier frequency of the baseband signal  $f_{cBB}$  and using  $f_{cBB} = f_{ctarget}/i$ , it comes:

$$i > 2f_{ctarget}/f_{smax} \quad (34)$$

For this case study, it gives  $i > 4.4$  with  $f_{smax} = 400MHz$ ,  $i > 5.3$  with  $f_{smax} = 330MHz$  and  $i > 7.3$  with  $f_{smax} = 240MHz$ . The first odd harmonic replica that can be exploited is therefore the 5<sup>th</sup>-order harmonic replica for  $f_{smax} = 400MHz$ , the 7<sup>th</sup>-order harmonic replica for  $f_{smax} = 330MHz$  and the 9<sup>th</sup>-order harmonic replica for  $f_{smax} = 240MHz$ .

The second step is to compute the parameters of the baseband signal according to the selected harmonic replica. The carrier

frequency of the baseband signal is simply given by the targeted carrier frequency divided by the order of the selected harmonic replica  $f_{cBB} = f_{ctarget}/i$ . In the same way, the modulation index of the baseband signal is given by the targeted modulation index divided by the order of the selected harmonic replica  $\beta_{BB} = \beta_{target}/i$ , the targeted modulation index being derived from the effective transmission band of the targeted modulated signal with  $\beta_{target} = B_{Ttarget}/2f_m - 1 = 0.653$ .

Once the baseband signal parameters are set, the next step is to identify favorable sampling conditions based on the corruption estimator. Practically, for each selected harmonic replica, the corruption estimator  $HRCE_i$  is computed varying the sampling frequency between a low limit determined by the Nyquist criterion  $f_{smin} = 2f_{ctarget}/i$ , and the upper limit  $f_{smax}$  imposed by the equipment, by step of  $2MHz$ . Valid solutions are then simply identified by selecting cases that give minimal corruption (with 2% tolerance on the minimal value). Table I summarizes the parameters of the baseband signal and the sampling frequency exploration range, according to the harmonic replica exploited for the generation of the targeted modulated signal.

TABLE I.  
BASEBAND SIGNAL PARAMETERS AND SAMPLING FREQUENCY EXPLORATION RANGE ACCORDING TO THE ORDER OF THE EXPLOITED HARMONIC REPLICA

		Harmonic replica order $i$		
		5	7	9
Baseband signal parameters	Carrier frequency $f_c$	17.36MHz	12.4MHz	9.644MHz
	Modulation index $\beta$	0.131	0.093	0.073
	Max freq. deviation $f_\Delta$	98kHz	70kHz	54.444kHz
$f_s$ exploration range	Minimum limit $f_{smin}$	348MHz	248MHz	194MHz
	Maximum limit $f_{smax}$	400MHz	330MHz	240MHz

Results of the exploration are summarized in Figure 19, which shows the attenuation factor of valid solutions. It can be observed that valid solutions exist for the three equipment constraints considered. However, their number significantly differs depending on the equipment constraint, i.e. 15 valid solutions for  $f_{smax} = 400MHz$ , 20 for  $f_{smax} = 330MHz$  and only 4 for  $f_{smax} = 240MHz$ . Two main factors contribute to this variance, namely the presence of a local zero due to the  $\sin_c$  function within the exploration range, and the size of the exploration range. The presence of a local zero within the exploration range limits the number of valid solutions since they cause harmonic replica cancellation, which is the case for  $f_{smax} = 330MHz$  and  $f_{smax} = 240MHz$  with local zeros located around  $217MHz$  and  $289MHz$  (sub-multiples of the targeted signal frequency). The size of the exploration range also has an impact on the number of valid solutions since it determines the number of explored solutions, i.e. 27 for  $f_{smax} = 400MHz$ , 42 for  $f_{smax} = 330MHz$  and 24 for  $f_{smax} = 240MHz$ .

A second comment is that valid solutions differ in terms of attenuation factor, with values comprised between  $30.7dB$  and  $34.9dB$  for the 5<sup>th</sup>-order harmonic replica,  $35.1dB$  and  $44.1dB$  for the 7<sup>th</sup>-order harmonic replica, and  $40.1dB$  and  $43.1dB$  for the 9<sup>th</sup>-order harmonic replica. For each harmonic replica, the

best solution is the one that minimizes the attenuation factor, i.e.  $f_s = 354\text{MHz}$  if  $f_{s\max} = 400\text{MHz}$ ,  $f_s = 328\text{MHz}$  if  $f_{s\max} = 330\text{MHz}$ , and  $f_s = 238\text{MHz}$  if  $f_{s\max} = 240\text{MHz}$  as summarized in Table II. Note that the sampling frequency of the retained solution is close to the maximum limit imposed by the equipment for the 9<sup>th</sup> and 7<sup>th</sup>-order harmonic replicas, but not for the 5<sup>th</sup>-order harmonic replica.

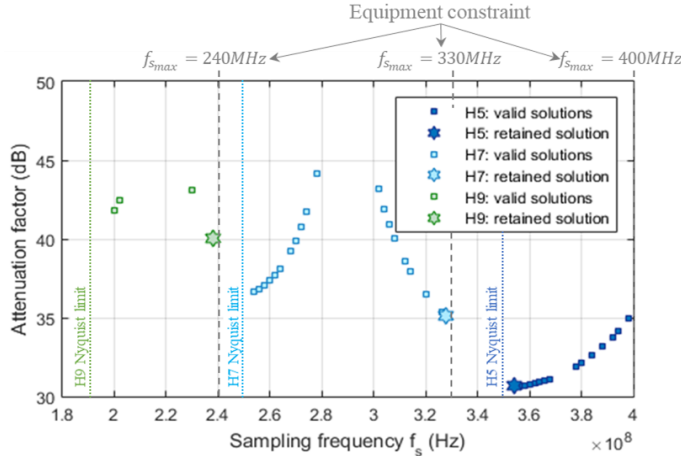


Fig.19. Illustration of valid sampling conditions under different constraints on the maximum sampling frequency allowed by the equipment.

TABLE II.  
RESULTS OF CORRUPTION ANALYSIS: RETAINED SAMPLING CONDITION  
ACCORDING TO THE EQUIPMENT FREQUENCY CAPABILITY

	Equipment constraint: $f_{s\max}$		
	400MHz	330MHz	240MHz
Harmonic replica order	5	7	9
# explored solutions	27	42	24
# valid solutions	15	20	4
Retained solution	$f_s = 354\text{MHz}$ $Att = 30.7\text{dB}$	$f_s = 328\text{MHz}$ $Att = 35.1\text{dB}$	$f_s = 238\text{MHz}$ $Att = 40.1\text{dB}$

### B. Hardware measurements

Hardware measurements were carried out to validate the settings determined from the corruption analysis. However, retained solutions cannot be directly implemented in the experimental test bench because the FM rate of our RF generator is limited to  $80\text{kHz}$ . We therefore apply a downscaling by 10 on all frequencies, i.e.  $f_{c\text{target}} = 86.8\text{MHz}$ ,  $f_m = 75\text{kHz}$  and  $B_{T\text{target}} = 248\text{kHz}$ . The downscaling factor is also applied on the retained sampling frequencies, i.e.  $f_s = 35.4\text{MHz}$  when working with the 5<sup>th</sup>-order harmonic replica under the assumption of an equipment limited to  $40\text{MHz}$ ,  $f_s = 32.8\text{MHz}$  when working with the 7<sup>th</sup>-order harmonic replica under the assumption of an equipment limited to  $33\text{MHz}$ , and  $f_s = 23.8\text{MHz}$  when working with the 9<sup>th</sup>-order harmonic replica under the assumption of an equipment limited to  $24\text{MHz}$ .

Results are presented in Figures 20, 21 and 22, which show the spectrum computed on the captured transient data (both global and close-up view around the selected harmonic replica), for the three equipment constraints considered. In all cases, the spectrum exhibits the desired modulation characteristics in the targeted transmission band without any significant unwanted components in the enlarged bandwidth, thus validating the implementation of the proposed approach. These results also confirm the adaptability of the approach, since it can deal with

different sampling frequency constraints imposed by the equipment by exploiting different harmonic replicas.

Finally for demonstration purposes, a solution whose sampling frequency is close to a retained solution, but which was not identified as a valid solution on the basis of the corruption estimator, was also implemented in the experimental test bench. Figure 23 shows the close-up view of the spectrum around the 7<sup>th</sup>-order harmonic replica when using a sampling frequency  $f_s \cong 33.0\text{MHz}$ . The components related to the desired modulation characteristics are indeed present in the targeted transmission band, but unwanted components are also at the edges of the signal bandwidth as well as in the extended bandwidth. This example clearly illustrates the effectiveness of the proposed corruption estimator in identifying favorable sampling conditions.

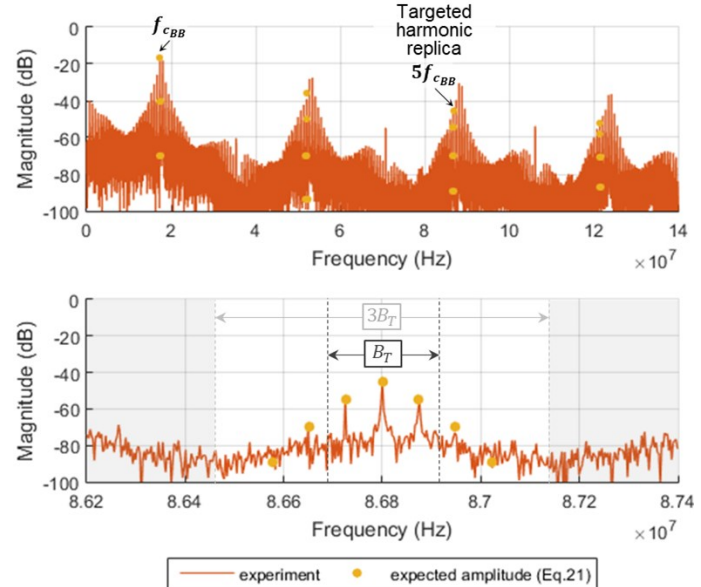


Fig.20. Modulated digital signal spectrum with  $f_{cBB} = 17.36\text{MHz}$  and  $f_s \cong 35.4\text{MHz}$  (signal generation based on 5<sup>th</sup>-order harmonic replica).

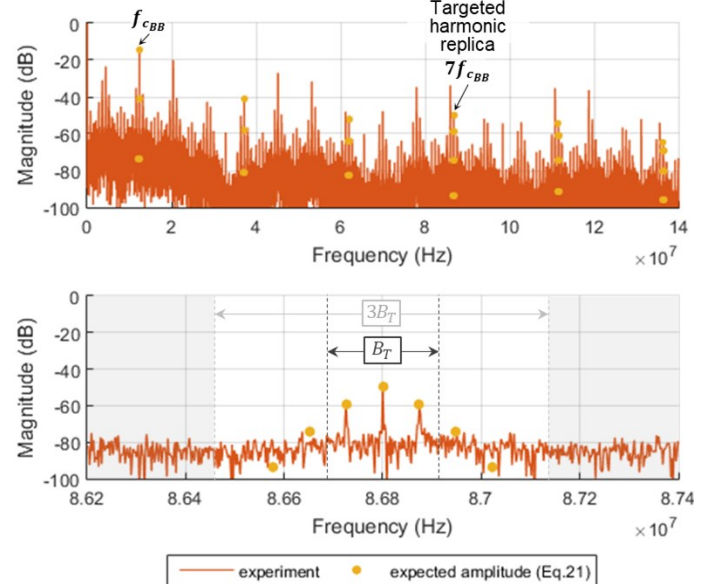


Fig.21. Modulated digital signal spectrum with  $f_{cBB} = 12.4\text{MHz}$  and  $f_s \cong 32.8\text{MHz}$  (signal generation based on 7<sup>th</sup>-order harmonic replica).

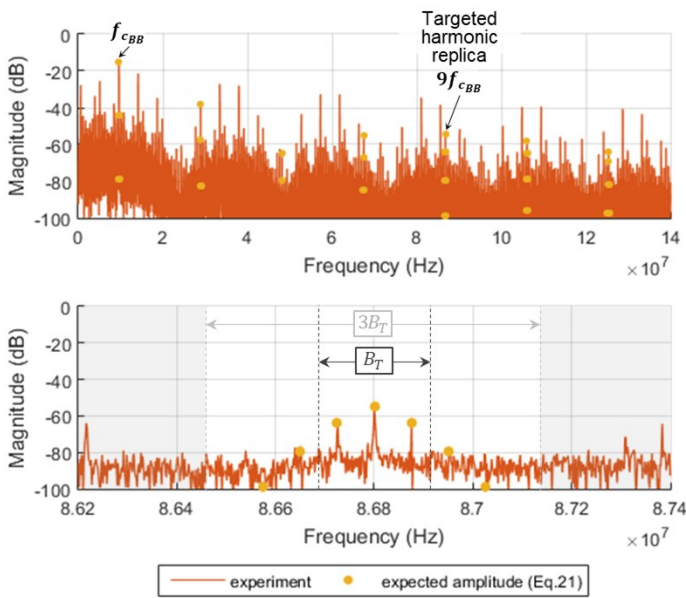


Fig.22. Modulated digital signal spectrum with  $f_{c_{BB}} \cong 9.644\text{MHz}$  and  $f_s \cong 23.4\text{MHz}$  (signal generation based on 9<sup>th</sup>-order harmonic replica).

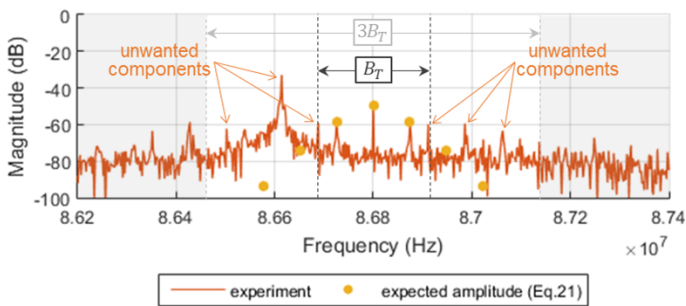


Fig.23. Illustration of a non-favorable sampling condition:  $f_s \cong 33.0\text{MHz}$  (signal generation based on 7<sup>th</sup>-order harmonic replica).

### C. Additional validation using only digital resources

An additional validation was carried out using only digital resources for the generation of the modulated test stimulus. For this, a new setup was developed based on the NXP Semiconductor's i.MX RT1170 evaluation board. As shown in Figure 24, the internal SRAM is used to store the binary sequence corresponding to the baseband modulated signal. This sequence is read by the Arm-Cortex-M7 core and the resulting signal is output on a high-speed GPIO (General-Purpose Input/Output) port. As in the previous setup, signal acquisition is performed by the oscilloscope at 25Gbps and captured transient data are transferred to a PC to compute the spectrum.

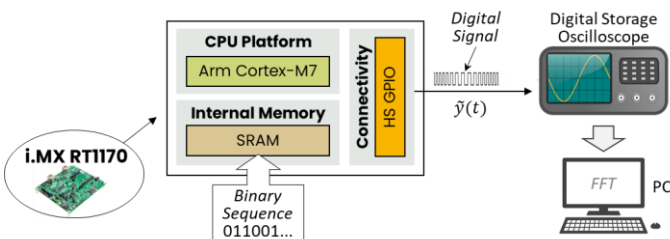


Fig.24. Hardware setup for validation of case study using digital resources.

The Arm-Cortex-M7 core can operate at up to 1GHz, which imposes a maximum constraint of 500MHz for reading the

sequence stored in the memory (two instructions are required to output each bit of the sequence on the GPIO port). With this constraint, the generation of an 868MHz modulated signal can be targeted using the 5<sup>th</sup>-order harmonic replica, choosing a bit rate  $f_s = 354\text{MHz}$  as established in section V.A. The operating frequency of the Arm-Cortex-M7 core is therefore set at 708MHz. The corresponding binary sequence stored in the memory is determined from the zero-crossed and sampled signal computed with the mathematical model defined in Figure 2.

Figure 25 shows the close-up view around the 5<sup>th</sup>-order harmonic replica of the spectrum computed on the captured digital signal. The spectrum exhibits the desired spectral characteristics in the targeted transmission band, i.e. a central component at 868MHz and two sideband components located 750kHz apart with an amplitude 11.9dB lower than that of the central component; no components of significant amplitude are present in the enlarged bandwidth.

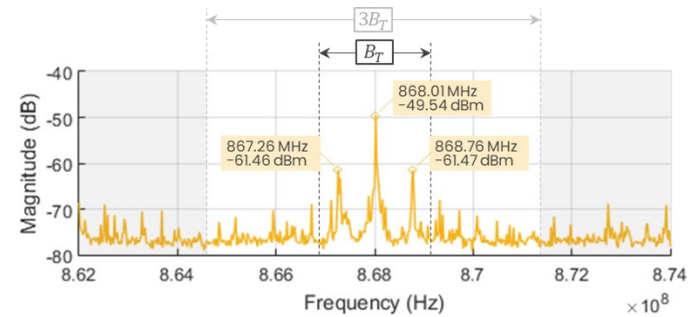


Fig.25. Experimental spectrum of the digital signal generated by reading the bit sequence stored in the SRAM at a bit rate of 354MHz.

This additional experiment confirms the validity of the proposed approach for obtaining RF modulated signals with specific characteristics from a digital signal generated at lower frequency.

## VI. CONCLUSION

In this paper, we have demonstrated a low-cost solution for generating FM/PM test stimuli in the RF range using a standard digital ATE. The proposed method uses spectral images of the binary signal generated by a digital tester channel in order to reach frequencies beyond Nyquist. The desired spectral characteristics are achieved through appropriate encoding of the digital sequence stored in the ATE and careful selection of the ATE sampling frequency. A theoretical analysis has been conducted, allowing to establish the relationship between the baseband spectrum and harmonic replicas in the continuous-time domain. The effects of sample-and-hold operations, which are representative of the operating mode of a digital ATE, have then been analyzed and an analytical expression of the modulated signal delivered by a digital tester channel has been derived. On the basis of this expression, a corruption estimator has been defined, which permits to identify non-destructive sampling conditions. The strategy has been evaluated through both simulation and hardware measurements. Results have validated the theoretical developments and the effectiveness of the corruption estimator in identifying favorable sampling conditions. Implementation on a practical case study has

demonstrated the ability of the proposed approach to generate good quality modulated FM/PM signals at a frequency higher than that of the test equipment. Future work will target extension to digital modulation formats used by actual receivers, such as Frequency-Shift Keying (FSK), Binary Phase-Shift Keying (BPSK), Quadrature Phase-Shift Keying (QPSK) and Minimum-Shift Keying (MSK), in order to enable low-cost testing of receiver sensitivity.

## REFERENCES

- [1] I. Kore, B. Schuffenhauer, F. Demmerle, F. Neugebauer, G. Pfahl and D. Rautmann, "Multi-site test of RF transceivers on low-cost digital ATE," IEEE International Test Conference (ITC), pp. 1-10 2011.
- [2] C. -H. Peng et al., "A novel RF self test for a combo SoC on digital ATE with multi-site applications," IEEE International Test Conference (ITC), pp. 1-8, 2014.
- [3] M. Ishida and K. Ichiyama, "An ATE System for Testing RF Digital Communication Devices With QAM Signal Interfaces," in IEEE Design & Test, vol. 33, no. 6, pp. 15-22, Dec. 2016.
- [4] N. Pous, F. Azaïs, L. Latorre, and J. Rivoir, 2011. "A Level-Crossing Approach for the Analysis of RF Modulated Signals Using Only Digital Test Resources," in J. of Electronic Testing: Theory and App. (JETTA), vol. 27, no. 3, pp 289-303, 2011.
- [5] S. David-Grignot, F. Azaïs, L. Latorre and F. Lefevre, "Low-cost phase noise testing of complex RF ICs using standard digital ATE," IEEE International Test Conference (ITC), pp. 1-9, 2014.
- [6] T. Vayssade, F. Azaïs, L. Latorre and F. Lefèvre, "Low-Cost EVM Measurement of ZigBee Transmitters From 1-bit Undersampled Acquisition," in IEEE Transactions on Computer-Aided Design of Integrated Circuits and Systems, vol. 40, no. 11, pp. 2400-2410, 2021.
- [7] H. Malloug, M. J. Barragan, S. Mir, E. Simeu and H. Le-Gall, "Mostly-digital design of sinusoidal signal generators for mixed-signal BIST applications using harmonic cancellation," IEEE International Mixed-Signal Testing Workshop (IMSTW), pp. 1-6, 2016.
- [8] S. David-Grignot, A. Lamlih, M. Moez Belhaj, V. Kerzérho, F. Azaïs, F. Soulier, P. Freitas, T. Rouyer, S. Bonhommeau, and S. Bernard, "On-chip "Generation of Sine-wave Summing Digital Signals: an Analytic Study Considering Implementation Constraints," in J. of Electronic Testing: Theory and App. (JETTA), vol. 34, no. 3, pp. 281-290, 2018.
- [9] A. Banerjee, S. K. Devarakond, V. Natarajan, S. Sen and A. Chatterjee, "Optimized digital compatible pulse sequences for testing of RF front end modules," IEEE 16th International Mixed-Signals, Sensors and Systems Test Workshop (IMS3TW), pp. 1-6, 2010.
- [10] M. A. Zeidan, G. Banerjee, R. Gharpurey and J. A. Abraham, "Phase-Aware Multitone Digital Signal Based Test for RF Receivers," in IEEE Transactions on Circuits and Systems I: Regular Papers, vol. 59, no. 9, pp. 2097-2110, Sept. 2012.
- [11] T. Vayssade, M. Chehaitly, F. Azaïs, L. Latorre and F. Lefevre, "Exploration of a digital-based solution for the generation of 2.4GHz OQPSK test stimuli," IEEE European Test Symposium (ETS), pp. 1-6, 2021.
- [12] K. Tahraoui, F. Azaïs, L. Latorre, F. Lefevre and T. Vayssade, "Digital generation of single-tone FM/PM test stimuli: a theoretical analysis," accepted at IEEE Latin-American Test Symposium (LATS), 2024.
- [13] M. Negreiros, A. Souza Jr., L. Carro and A. A. Susin, "RF Digital Signal Generation Beyond Nyquist," IEEE VLSI Test Symposium (VTS), pp. 15-22, 2007.
- [14] S. Haykin, "An Introduction to Analog and Digital Communications", 2<sup>nd</sup> Edition, Wiley & Sons, 2006.



**K. Tahraoui** received the M.S. degree in Electrical Engineering from the University of Montpellier, France, in 2020.

She is currently a Ph.D. student at LIRMM, Montpellier, France. She works on the development of low-cost digital test solutions for RF devices.



**T. Vayssade** received M.S. and Ph.D. degrees in Electrical Engineering from the University of Montpellier, France, in 2017 and 2020 respectively.

From 2021 to 2023, he was an electronic engineer at ELA Innovation, France. He is now an associate professor at the University of Montpellier, France. His main research

interests are RF testing and signal processing.



**F. Lefèvre** received the Engineer's degree with radio-frequency option from the ENSERG engineering school of Grenoble, France, in 1994.

He is currently with NXP Semiconductors, Caen, France. He leads the Design for Test definition of large RF, mixed-signal and

digital ICs activities, together with the industrial test development tasks.



**L. Latorre** received the M.S. degree in Mechanical and Electronic Engineering from the University of Montpellier, France, in 1995 and the Ph.D. degree in Electrical Engineering from the University of Montpellier, France, in 1999.

He is currently head of the Microelectronics department at LIRMM, Montpellier, France. His main research interests are low-power embedded systems, signal processing, test, and integrated front-end electronics for sensors.



**F. Azaïs** received the M.S. and Ph.D. degrees in Electrical Engineering from the University of Montpellier, France, in 1993 and 1996 respectively.

She is currently a CNRS researcher at LIRMM, Montpellier, France. Her main research interests are AMS/RF circuit testing, and reliability of integrated systems.